

ACETIC ACID AND CARBON DIOXIDE CORROSION OF CARBON STEEL COVERED WITH IRON CARBONATE

Egil Gulbrandsen
Institute for Energy Technology
Instituttveien 18
NO-1254 Kjeller, Norway

ABSTRACT

Acetic acid and CO₂ corrosion was investigated on carbon steel specimens covered with iron carbonate (FeCO₃) layers. The tests were carried out at 80 °C, 0.5 bar CO₂, using rotating cylinder electrodes. Protective iron carbonate layers did form in solutions with high FeCO₃ supersaturation, both in presence and absence acetic acid. The protective effect of the FeCO₃ layer failed with decreasing supersaturation. The results were interpreted in terms of the scaling tendency concept.

Key words: acetic acid, carbon dioxide, corrosion, carbon steel, iron carbonate

INTRODUCTION

Short chain carboxylic acids are often present in oil and gas reservoirs beside other corrosive compounds like carbon dioxide (CO₂) and hydrogen sulfide (H₂S). Amongst these short chain acids, acetic acid (CH₃COOH, abbreviated HAc) appears to be the most abundant. A systematic investigation of field data showed that undissociated HAc concentration higher than 0.1-1 mM was a critical factor for corrosion.¹ The corrosion failures were always caused by localized attack (mesa type of attack). It was pointed out that localized corrosion necessarily involved surface deposits (protecting the surrounding areas, but not in the localized attack).

The literature on the effect of HAc on CO₂ corrosion was recently reviewed.² The reviewed literature show that HAc can give a significant contribution to the overall corrosion rate, and raise the uninhibited corrosion rate to several tens of millimeters per year. There seems to be an agreement that HAc can increase the cathodic reaction rate (hydrogen evolution reaction) if the concentration is significant. The corrosion rate can then be correlated to the concentration of undissociated HAc present in the brine. Equilibrium calculations involving all species and reactions in the system are therefore

essential to understand test results and predict the corrosiveness in the field from produced water analyses. The three main cathodic reactions appear to be³⁻⁴



where the rate of reaction (3) may be limited by the preceding slow hydration of CO_2 :³



Equations (1)-(3) reflect overall reaction, and do not purport to indicate detailed mechanisms of the proton reduction. The relative contribution from each of these reactions routes depends on the concentrations of the reacting species, temperature, pH, and convection. The H_2 evolution from HAc seems to be under activation control.²⁻³

The reaction mechanism and kinetics of the iron dissolution reaction, with the overall reaction



are affected by acetic acid,⁵ in addition to CO_2 partial pressure and pH.⁶ It seems established that HAc or Ac^- may retard the anodic part reaction,^{2,5} This effect was in particular observed at room temperature, where it lead to a slight reduction in general corrosion rate, but increased the tendency of localized attack.²

Iron carbonate (FeCO_3) forms when the solubility product K_{sp} is exceeded. The overall reaction is



The relative supersaturation (S_r), defined by

$$S_r = ([\text{Fe}^{2+}][\text{CO}_3^{2-}]) / K_{\text{sp}} \quad (7)$$

is an important parameter for film growth. It is calculated from measured Fe^{2+} concentrations, and CO_3^{2-} concentrations calculated from pH and CO_2 concentrations using well-known thermodynamic data. The growth rate of FeCO_3 depends strongly on the supersaturation and the temperature, see Discussion section.

In summary, a number of factors appear to determine the corrosion rate in presence of HAc and CO_2 . These factors include:²

- Concentration of the reactants and products
- Electrochemical kinetics of cathodic reactions

- Electrochemical kinetics of the anodic reaction(s) (inhibition by HAc, localized or uniform dissolution)
- Corrosion product films (kinetics of formation and morphology)

While significant progress has been made in the understanding of the three first bullet points on bare steel surfaces, little work has yet been done on the behavior of corrosion product films in systems with HAc present.

Formation of FeCO_3 corrosion films in pure CO_2 environments has, however, been studied both experimentally and theoretically.⁷⁻¹⁶ Many of the authors adopt the scaling tendency concept proposed by van Hunnik et al.⁹ This concept, which focuses on the competition between FeCO_3 film growth and corrosion, gives a description of FeCO_3 film growth and protectiveness that is consistent with many experimental findings. The Scaling Tendency (ST) is defined as the ratio between the corrosion film growth rate and the corrosion rate. Thus, with $\text{ST} > 1$, the film growth rate is faster than the corrosion rate; the corrosion deposit will cover the steel surface and reduce the corrosion rate until a steady rate is reached. If, on the other hand, ST is lower, the metal corrodes faster than the corrosion film can grow, and no protectiveness is obtained. The scaling tendency concept implies that corrosion can take place in voids underneath a porous FeCO_3 film. Nesic and coworkers¹¹⁻¹³ developed a mechanistic CO_2 corrosion model that accounts for the effect of FeCO_3 corrosion films. These authors distinguish between bulk ST, which refers to the bulk solution conditions, and the surface ST (SST), which refers to the actual conditions at the metal surface.¹² By means of numerical modeling and experiments they reached the conclusion that protective (FeCO_3) films reduce the corrosion rate primarily by blocking the metal surface rather than by reducing the diffusion of corrosive species. As a consequence of this, detached films had poor protective properties even when they were very dense. Diffusion of dissolved CO_2 was found to be the main mechanism of providing reactants to the corrosion reaction at the metal surface.¹²

Regarding systems with HAc and CO_2 , Dugstad and co-workers¹⁷ tested the effect of 12 ppm undissociated HAc under film forming conditions at 80 °C. (Flow loop, 2 bar CO_2 , pH 5.8, 6-30 ppm Fe^{2+} (i.e. supersaturated), 0.1 % NaCl. The total amount of acetic species was 90-120 ppm. The corrosion attack varied considerably between the different steels tested. However, it was concluded that the HAc caused more mesa attack (high number of small attacks). The corrosion films were more fragmented, with more pores and flaws. In some cases a protective corrosion film did not form at all. The localized corrosion was more severe at high flow rates.

Furthermore, Nafday and Nesic¹⁸ studied the effect of HAc on FeCO_3 corrosion product film protectiveness at 80 °C in 3 wt-% NaCl under 0.5 bar CO_2 . The concentration of undissociated HAc was in the range 0-180 ppm. The tests were carried out at relative FeCO_3 supersaturations equal to 32 and 162. No significant effect of HAc on FeCO_3 layer protectiveness or morphology was found in any of the tests. The corrosion film growth rate, inferred from the rate of decrease of corrosion rate, was determined by the supersaturation.

Crolet and Bonis¹⁹ recently discussed the effect of HAc on pH and FeCO_3 solubility and points out that acetic acid in low concentrations decreases the solubility of FeCO_3 and thus increases the risk of localized corrosion attack. These authors argue against the scaling tendency concept. The main objections are that a corrosion layer is attached to the steel surface, and cannot be undermined by corrosion to “float alone in space”, and that a FeCO_3 film cannot grow at the metal/film interface in a steady state situation.

The present paper reports the results of a laboratory study on the effect of HAc under conditions with formation of corrosion product films at 80 °C. The objective of the work was to assess the effect of HAc on the formation and protectiveness of corrosion films of iron carbonate (FeCO₃).

EXPERIMENTAL METHOD

Test solutions were prepared from distilled water, analytical grade HAc and reagent grade NaCl. The Fe²⁺ rich replenishment solutions were prepared by corroding commercially available steel wool in the brine under 1 bar CO₂ atmosphere at 50 °C. The steel wool was degreased in acetone prior to use.

The rotating cylinder test specimens (10 mm diameter, 10 mm height, 3.14 cm² exposed area) were machined from X65 pipeline steel. The elemental analysis and microstructure of the steel used are given in Table 1. The test specimens were pre-treated by grinding with 1000 mesh SiC paper wetted with isopropanol, and degreasing in acetone.

Corrosion was studied electrochemically by use of a commercially available potentiostat equipped with an eight-channel multiplexer. A three-electrode configuration was used in all the measurements. The tip of a carbon steel wire was used as reference electrode for the potentiostat. The wire was insulated by a PTFE hose; only the end of the wire was exposed to the solution. Corrosion rates were determined from polarization resistance,²⁰ which was measured by a 0.1 mV/s potential scan from -5 to +5 mV vs. the corrosion potential. A conversion factor B=20 mV was used to calculate corrosion rate from polarization resistance. This value of B is in agreement with previous experience from CO₂ and HAc corrosion.^{2,4,21}

The interval between the measurements was in most cases 60 minutes. The parameters used for electrochemical measurements and corrosion rate calculations are summarized in Table 2. A data logger was used to monitor the corrosion potential of the specimen vs. the Ag/AgCl (3 M KCl) reference half-cell of the combination pH electrode. This logger also recorded the cell temperature and the solution pH. The logging frequency was synchronized with the potentiostat, logging the corrosion potential a few minutes before each polarization resistance scan. Potentiodynamic scans were performed at the end of the test. All the reported results were corrected for uncompensated electrolyte resistance determined by electrochemical impedance spectroscopy.

A schematic drawing of the test set-up is shown in Figure 1. A peristaltic pump brought the test solution from the reservoir (a 25-litres HDPE tank) to the test cell. The flow rate was 1 liter/h. A magnetic stirrer was used to keep the solution properly mixed in the test cell. An overflow pipe maintained a constant liquid volume in the cell. The liquid discharged from the cell was collected in a drain tank. The reservoir tank and the test cell were continuously purged with CO₂. Water-cooled reflux condensers were mounted at the gas outlets of the reservoir and test cell in order to minimize loss of water and HAc. The discharge gas and liquid were passed through water locks to avoid air ingress. The temperature was controlled by means of a heating plate fitted with a temperature sensor in the cell. An enclosure was built around the rotating cylinder electrode motor. This enclosure was purged with dry CO₂ gas to minimize ingress of water vapor to the bearings and contacts.

The test solution was prepared in the 25 liters reservoir tank. The accuracy of the concentrations was within 2 % relative error. The FeCO₃ supersaturated solutions were prepared by adding steel wool corresponding to 450 ppm Fe²⁺ to the reservoir barrel. The steel wool was allowed to corrode for 2-3 days at 50 °C under CO₂ atmosphere. Iron(II) concentration was determined by spectrophotometry at 508 nm as ortho-phenanthroline complex. The analyses confirmed that essentially all the steel wool had

corroded. The reservoir barrel was held at room temperature during the test. No significant precipitation of FeCO_3 in the reservoir barrel was detected, neither by iron counts, nor by visual inspection. The main reason for this is assumed to be the low precipitation rate of FeCO_3 at room temperature, see Discussion section. Furthermore, the solubility of FeCO_3 increases with decreasing temperature, thus reducing the supersaturation.

Equilibrium concentrations of HAc were calculated from measured pH using the equilibrium constants given in Table 3.

RESULTS

In these tests supersaturated test solution was continuously replenished from the reservoir. The rotation rate was kept constant at 100 RPM in all the tests. Figure 2 shows the results of a test where the total acetate concentration was increased stepwise. The test was started with no HAc in the solution. The relative supersaturation (S_r) was about 100.* The corrosion rate dropped below 0.1 mm/y in one day as a result of the formation of a protective FeCO_3 film. After 2 days exposure, a total of 60 ppm acetic species (measured as HAc equivalents) was added to the replenishment solution.# The free HAc concentration was ca. 4 ppm (calculated from pH data, see Fig. 2b-c). The ratio of acetic acid to sodium acetate was chosen to give approximately the same pH in the test cell as before the change. The corrosion rate was not significantly affected by the change in solution composition; the corrosion rate continued to decrease slowly towards 0.01 mm/y after 4 days. The corrosion potential (E_{cor}) increased from -0.67 V to -0.59 V during this period.

After 4.5 days exposure the solution replenishment stopped for 1.5 days. The iron concentration dropped from 150 ppm to 50 ppm due to further FeCO_3 precipitation on the glass walls of the cell. S_r decreased to ca. 1 after 6 days, and the corrosion rate increased to 0.5 mm/y during this period. E_{cor} decreased to -0.66 V during this period. An iron count at 5 days showed that a S_r value of 13 was not enough to maintain the protectiveness of the film, since the corrosion rate was already increasing at that stage.

After 6 days of testing the solution replenishment was restarted, now with a solution containing 600 ppm of acetic species (ca. 100 ppm HAc). The corrosion rate started to decrease again, and E_{cor} increased. S_r had now increased to 30-40 due to the replenishment with Fe^{2+} rich solution. The test solution was changed to 6000 ppm total acetic species after 8 days (with order of 1000 ppm free HAc). At such high acetate concentration, formation of ferrous acetate complex, FeAc^+ , caused a reduction in Fe^{2+} , thus giving a decrease in S_r to ca. 10, see equilibrium calculations reported in Ref. 2. The corrosion rate rapidly increased to 1-2 mm/y and fluctuated between 0.5 and 1 mm/y until 12 days. The E_{cor} dropped to a low level again.

After 12 days exposure the pH was increased slightly by addition of sodium hydroxide (NaOH). The corrosion rate went down to about 0.2 mm/y. Since S_r is proportional to $[\text{Fe}^{2+}]/[\text{H}^+]^2$ the decrease in $[\text{H}^+]$ is expected to dominate over the decrease in $[\text{Fe}^{2+}]$ caused by increased complex formation at higher pH. With 60 - 600 ppm acetic species the ferrous acetate complex formation is less pronounced,²

* S_r is calculated from bulk solution conditions, not actual surface conditions.

#The new solution was pumped with a rate of ca. 1 litre/h into the 2.5 litre cell. This gave a time constant of ca. 2.5 h for the exponential rate of change of concentration in the test cell when the concentration in the reservoir solution was changed. That is, about 95 % of the change was completed in 7.5 h.

and caused only minor changes in S_r . SEM investigation showed ca. 20 μm porous film, the crystallites appeared to have a platelet morphology.

In summary, this test showed that it was possible to maintain protective FeCO_3 films at 80 °C in presence of up to a least 100 ppm free HAc, provided the relative supersaturation was about 30 times or higher. Protection was lost below this value. The test results with 6000 ppm total acetic species were consistent with this when the supersaturation was corrected for the substantial formation of ferrous acetate complex.

Figure 3 shows the results of another test where solution replenishment was stopped in order to observe the effect of decreasing the supersaturation. This test was performed in the absence of acetic species. The corrosion rate decreased with time to about 0.01 mm/y after 3.7 days of exposure with continuous replenishment of supersaturated test solution. The relative supersaturation in the test cell decreased with time to about 100 during this period, as a result of FeCO_3 precipitation at all the surfaces in the cell. When the solution replenishment was stopped after 3.7 days the relative supersaturation decreased to ca. 1 (saturation point) in about 1 day, and the corrosion rate increased rapidly, approaching 1 mm/y. E_{cor} followed a similar pattern as in Figure 2, i.e. increased when the corrosion rate decreased due to film formation, and decreased as a result of the loss of protection. Optical microscopy showed that a crystalline corrosion film covered the specimen. SEM cross sections showed that the 10-20 μm thick, dense film was detached from the steel in most parts of the specimen. The corrosion behavior thus resembles the one in Figure 2.

In the two previous tests the FeCO_3 film was initially formed in the absence of acetic acid. In Figure 4, HAc was present in the test solution from the start of the test, to see if this modified the film formation. The total concentration of acetic species was 60 ppm, the concentration of undissociated HAc was ca. 3 ppm. The corrosion rate decreased to 0.01 mm/y after 4 days. Evidently a protective corrosion film was formed. The value of S_r started at 330, but dropped to 135 at the end of the test as a result of FeCO_3 precipitation in the cell. E_{cor} increased with decreasing corrosion rate to about -0.56 V. The SEM investigation showed a 100 μm porous film that was built up from randomly oriented platelet crystallites.

In the next test (Figure 5), the total acetic species concentration was raised to 600 ppm, and the undissociated HAc concentration was 70-120 ppm. S_r was initially about 100, and decreased with time to 25-30. The corrosion rate decreased to 0.03 mm/y after 5 days. The protective film formation was thus slower in this test than in the previous test with no HAc initially (Figs. 2-3). Solution replenishment was stopped after 5.6 days. S_r dropped to ca. 20, and the corrosion rate started to increase, while E_{cor} decreased. SEM examination showed a relatively dense, crystalline 20-30 μm film that was partly detached from the surface. The inner part of the film was in close contact with the metal.

In summary, the tests with the rotating cylinder electrode at 80 °C showed consistently that the protective properties of the corrosion film was maintained whenever S_r was higher than 20-30. In the tests without HAc, protective film formation was initiated with S_r of 300 or more (Fig. 2-3). In the test with 60 ppm total acetic species protective film formation was also initiated with S_r of about 300 (Fig. 4). In the test of Figure 5 (with 600 ppm acetic species) protective film formation was apparently initiated at $S_r \approx 100$.

DISCUSSION

The tests at 80 °C show that protective FeCO₃ corrosion films can form, and remain protective in presence of acetic acid provided FeCO₃ supersaturation is high enough. This finding is in agreement with the conclusions of Nafday et al.¹⁸ The amount of data is, however, not sufficient to establish a critical value of S_r, above which protective films would form. With the present test protocol, the initiation of protective film formation may depend on a high peak in supersaturation in the early stage of the test. The present results do not provide sufficient details to analyze such effects. Small differences in time needed to reach 80 °C and insert the specimen may thus have influenced the initiation of film formation, since the Fe²⁺ concentration decreased rapidly the first period. Finally, protective films may form in the long run at lower supersaturation than observed in the present short-term tests.

The results indicate clearly, however, that relative FeCO₃ supersaturation is an important factor for film growth and the protectiveness of the film. This means that if acetic acid has a specific effect on the corrosion films, one has to go beyond the effects of supersaturation to study it.

The scaling tendency model⁹⁻¹³ gives a description of film growth and protectiveness that is consistent with most of the experimental findings in the present project. If the growth rate of the corrosion film is too low, the corrosion will move the metal surface faster than the corrosion film can follow, causing undermining of the corrosion film and loss of protectiveness.

The growth rate of FeCO₃ depends on the supersaturation. There are presently some discrepancies between the reported growth rates of FeCO₃. A recent paper²² reports significantly lower rates than two previous papers^{7,9}. Here the rate equation of van Hunnik et al.⁹ is used as an example to illustrate the temperature dependence:

$$d[\text{Fe}^{2+}]/dt = k_r (A/V) K_{sp} (S_r - 1)(1 - S_r^{-1}) \quad (8)$$

Here $d[\text{Fe}^{2+}]/dt$ is the Fe²⁺ precipitation rate in units of mole/(m³ s), k_r is the rate constant, A/V is the surface area to volume ratio, K_{sp} is the solubility product (in molality units, mole²/kg²), and S_r is relative supersaturation (Eq. 7). The rate constant, in units of kg²/(mole m² s), depends on temperature according to the Arrhenius equation:

$$k_r = \exp(B - E/RT) \quad (9)$$

B and E are experimentally determined constants:⁹ $B = 52.4$ and $E = 119.8$ kJ/mole (the activation energy), T is temperature (K), R is the universal gas constant.

Rearranging Eq. 8 gives the precipitation rate per unit area (mole/m² s)

$$(V/A) d[\text{Fe}^{2+}]/dt = k_r K_{sp} (S_r - 1)(1 - S_r^{-1}) \quad (10)$$

which leads to the FeCO₃ growth rate GR in units of meters per second

$$GR = (M/\rho) k_r K_{sp} (S_r - 1)(1 - S_r^{-1}) \quad (11)$$

Here M and ρ are the molar mass (0.116 kg/mole) and density (3.8×10^3 kg/m³), respectively, of FeCO₃.

The scaling tendency (ST) is defined as the ratio between the growth rate (GR) and the corrosion rate CR (expressed in the same units):

$$ST = GR/CR \quad (12)$$

The growth rate given by Eq. 11 is plotted in mm/y as a function of supersaturation in Figure 6a. The molarity (mole/litre) based solubility product listed in Table 3 was assumed to be equal to the molality based (mole/kg) one at moderate salt concentrations. The growth rate is proportional to S_r at high supersaturation. At supersaturation below ca. 10 the growth rate has a much stronger dependence on S_r .

It is well known that the temperature is an important factor for growth of protective films. According to Figure 6a, the growth rate is nearly 200 times higher at 80 than at 25 °C. The worst case corrosion rate increases only a few times from 25 to 80 °C. Accordingly, the scaling tendency concept explains why protective corrosion films form more easily at higher temperatures.

Literature data⁹⁻¹⁰ suggest that protective corrosion films do form when the scaling tendency exceeds a critical value of ca. 0.4-0.7, depending on experimental conditions and type of steel.

The scaling tendencies at different relevant corrosion rates are plotted as a function of relative supersaturation in Figure 6b. The experimentally estimated levels of supersaturation needed to maintain a protective film were the order of 10-30. These values give higher scaling tendencies than the critical values reported in the literature. Experimental error sources include suspended $FeCO_3$ particles possibly being included in the iron counts, and possible drift in pH electrode response due to $FeCO_3$ precipitation at the glass membrane. Furthermore, it should be noted that some disagreement exist concerning the film growth rate.^{7,9,22} Finally, calculated film growth rates are very dependent on the value of the $FeCO_3$ solubility product. For example, the value changes considerably with ionic strength.

The cause of the rise in corrosion rate from 0.01 to nearly 1 mm/y upon stopping the solution replenishment (Figs. 2-3) is obviously not due to dissolution of the corrosion film (since the solution is all the time saturated or supersaturated). The observations appear to be consistent with the scaling tendency model. The supersaturation decreased rapidly when the replenishment stopped due to $FeCO_3$ precipitation on all the surfaces in the cell. The protective properties of the film were lost when supersaturation decreased below a certain level, i.e. the corrosion rate exceeded the film growth rate at the metal surface and the film was detached (undermined) by corrosion of the steel. The rate of the process is surprisingly fast, however, considering the low LPR corrosion rate in the protective condition.

The molar volume of $FeCO_3$ is about twice that of metallic Fe. The growth of $FeCO_3$ at the metal surface is therefore likely to produce a film with considerable amount of internal stress. It is not likely that the $FeCO_3$ crystals will grow only in the direction normal to the surface. The crystallites are likely to be randomly oriented on the polycrystalline steel surface, and thus grow in all directions from the surface. One may therefore speculate whether the stress that is likely to be present in the film at the metal surface may promote film detachment. At high ST a crack in the film would be rapidly healed. At low ST a crack could increase the LPR corrosion rate significantly. The postulated corrosion and stress detachment processes may even amplify each other. Such a combined detachment mechanism might therefore explain the rapid loss of protection and the decrease in corrosion potential observed in Figures 2-3.

The results presented in Figure 2-3 furthermore indicate that the detached films were not substantial barriers to the diffusion of CO₂, since the corrosion rate increased towards 1 mm/y when the supersaturation was decreased. This is in line with the conclusions of ref. 12. This behavior is a consequence of the chemistry of CO₂. It is highly soluble in water (e.g. 0.55 g/L, 12 mmol/L under 1 bar CO₂ at 80 °C). The H₂CO₃ concentration is only a small fraction (ca. 1/600) of the dissolved CO₂ concentration. Comparison of H₂CO₃ consumption rates and potential CO₂ diffusion rates show that only a small CO₂ concentration gradient arises through the diffusion layer in order to supply the consumption of H₂CO₃ via the hydration reaction (Eq. 4). Model calculations showed that even for a 50 μm thick FeCO₃ film with 1% porosity, the CO₂ concentration only decreased about 1% (relatively) through the film.¹²

The diffusion of Fe²⁺ and HCO₃⁻ from the surface, however, needs steeper concentration gradients. This leads to higher supersaturation, and thus higher FeCO₃ growth rates, at the metal surface than predicted using bulk solution conditions. Surface scaling tendency (SST) was therefore recently introduced as a parameter.¹² Furthermore, the higher the Fe²⁺ concentration in the bulk, the higher the supersaturation will be at the surface (with other parameters being the same).

The present results stress the importance of supersaturation for protective film formation. Other factors, like the initial presence of mill scales and rust films in carbon steel piping, and the much longer time-scale of film formation, may also be important factors that affect protective corrosion film in the field. Furthermore, variations in supersaturation may be caused by variation in temperature due to varying production rate. Thermodynamic considerations show that HAc decreases FeCO₃ supersaturation by lowering the pH of the brine, increasing the buffer capacity, and by formation of ferrous acetate complexes (at high acetate concentration). The effect HAc on surface S_r and scaling tendency should be studied in further work. It appears that long-term tests at conditions closer to the critical scaling tendency might be needed to assess the effect of small amounts of HAc in more detail.

The SEM examination showed that some of the specimens had corrosion films that were built from small randomly stacked platelet crystallites. These films, which appeared to be rather porous, were mostly observed in tests where HAc was present. This platelet film morphology was also seen in some tests with HAc in Ref. 17. The same report states that “the corrosion films were more fragmented, with more pores and flaws”. This was also noted in several of the tests in the present project. These observations may indicate that HAc or Ac⁻ modifies the morphology of the corrosion films. However, the data are too few to make conclusions at the present stage.

SUMMARY AND CONCLUSIONS

The rotating cylinder tests were performed at 80 °C with 0.5 bar CO₂. The test solution was continuously replenished with brine that was supersaturated with FeCO₃ (ca. 400 ppm Fe²⁺). However, FeCO₃ precipitated on all the surfaces in the cell, and it was difficult to maintain a constant high level of supersaturation.

- Protective corrosion films were formed at high supersaturation (S_r order of 100 or more), both in absence and presence of HAc.

The present amount of data is, however, not sufficient to establish a critical value of S_r, above which protective films would form. The initiation of protective film formation may depend on a high peak in supersaturation in the early stage of the test. Furthermore, protective films may form in the long run at lower supersaturation than observed in the present short-term tests.

- The tests showed consistently that the protective properties of the corrosion film was maintained when S_r was higher than 10-30. When the supersaturation dropped below this value the corrosion rate increased, even if the film did not dissolve (since the solution was still supersaturated).

The results were explained in terms of the scaling tendency model.⁹⁻¹⁴ In this model, the growth rate of the FeCO_3 film is considered. The FeCO_3 growth rate increases with increasing supersaturation. When the supersaturation decreased below a certain value, the corrosion rate could be faster than the film growth rate. The film could be detached by the corrosion and possibly by cracking of the film, and protection could be lost.

The results of the tests with film forming conditions stress the importance of supersaturation and temperature for protective film formation. Other factors, like the initial presence of mill scales and rust films in carbon steel piping, and the longer time-scale of film formation, may also be important factors that contribute to protective corrosion film in the field.

ACKNOWLEDGEMENT

The present work was a part of IFE's Joint Industry Project "Kjeller Acetic Acid Project" (1999-2002). The project was funded by BP, ENI Agip, Hydro, Shell, Statoil, and TotalFinaElf.

REFERENCES

1. M.R. Bonis, J.-L. Crolet, "Basics of the Prediction of the Risk of CO_2 Corrosion in Oil and Gas Wells", CORROSION/89, Paper no. 466, (Houston, TX: NACE International, 1989).
2. E.Gulbrandsen, K.Bilkova, "Solution Chemistry Effects on Corrosion of Carbon Steel in Presence of CO_2 and Acetic Acid", CORROSION/2006, Paper no. 06364, (Houston, TX: NACE International, 2006).
3. Y. Garsany, D. Pletcher, D. Sidorin, W.M. Hedges, Corrosion, 60, 1155 (2004).
4. S. Netic, J. Postlethwaite, S. Olsen, Corrosion, 52 (1996), p. 280.
5. J.-L. Crolet, N.Thevenot, A. Dugstad, "Role of free acetic acid on the CO_2 corrosion of steels", CORROSION/99, Paper no. 024, (Houston, TX: NACE International, 1999).
6. S.Netic, N.Thevenot, J.-L.Crolet, D.M.Drazic, "Electrochemical properties of iron dissolution in the presence of CO_2 - Basics revisited", CORROSION/96, Paper no. 3, (Houston, TX: NACE International, 1996).
7. M.L.Johnson, M.B.Tomson, "Ferrous Carbonate Precipitation Kinetics and its Impact on CO_2 Corrosion", CORROSION/91, Paper no. 268, (Houston, TX: NACE International, 1991).
8. A.Dugstad, "The importance of FeCO_3 supersaturation on the CO_2 corrosion of carbon steels", CORROSION/92, Paper no. 14, (Houston, TX: NACE International, 1992).
9. E.W.J.van Hunnik, B.F.M.Pots, E.L.J.A.Hendriksen, "The formation of protective FeCO_3 corrosion product layers in CO_2 corrosion", CORROSION/96, Paper no. 6, (Houston, TX: NACE International, 1996).

10. B.F.M.Pots, E.L.J.A.Hendriksen, "CO₂ corrosion under scaling conditions – The special case of top-of-line corrosion in wet gas pipelines", CORROSION/2000, Paper no. 031, (Houston, TX: NACE International, 2000).
11. M.Nordsveen, S.Nesic, R.Nyborg, A.Stangeland, Corrosion, 59 (2003), p. 443.
12. S.Nesic, M.Nordsveen, R.Nyborg, A.Stangeland, Corrosion, 59 (2003), p. 489.
13. S.Nesic, K-L.J.Lee, Corrosion, 59 (2003), p. 616.
14. S.Nesic, K-L.J.Lee, V.Ruzic, "A mechanistic model of iron carbonate film growth and the effect on CO₂ corrosion of mild steel". CORROSION/2002, Paper no. 237 (Houston, TX: NACE International, 2002).
15. V.Ruzic, M.Veidt, S.Nesic, Corrosion, 62 (2006), p. 419.
16. V.Ruzic, M.Veidt, S.Nesic, Corrosion, 62 (2006), p. 598.
17. A. Dugstad, H. Hemmer, H.Kooyman, W. Wilhelmsen, "Kjeller Sweet Corrosion III – Final report", IFE report no. IFE/KR/F-93/091, Institute for Energy Technology, (1993) (Restricted)..
18. O.A. Nafday, S. Nesic, "Iron Carbonate Scale Formation and CO₂ Corrosion in the Presence of Acetic Acid", CORROSION/2005, Paper no. 295, Houston, TX: NACE International, 2005).
19. J.-L. Crolet, M.R. Bonis, "Why So Low Free Acetic Acid Thresholds in Sweet Corrosion at Low P(CO₂)", CORROSION/2005, Paper no. 272, (Houston, TX: NACE International, 2005).
20. M. Stern, A.L. Geary, J. Electrochem. Soc., 104 (1957), p. 56.
21. E.Gulbrandsen, J.Kvarekvål, H.Miland, "Effect of Oxygen Contamination on Inhibition Studies in CO₂ Corrosion", Corrosion, 61, 1086 (2005).
22. K. Chokshi, W. Sun, S. Nesic, CORROSSION/2005, Paper no. 285, (Houston, TX: NACE International, 2005).
23. J.E. Oddo, M.B. Tomson, "The prediction of Scale and CO₂ Corrosion in Oil Field Systems", CORROSION/99, Paper no. 41, (Houston, TX: NACE International, 1999).
24. Institute for Energy Technology, In-house solubility calculation model, SOL18 (2001).

Table 1. Element analysis (wt-%) for the carbon steel specimens. Microstructure: Ferrite-pearlite.

Steel*	C	Si	Mn	S	P	Cr	Ni	V	Mo	Cu	Al	Sn	Nb
X65 (#57)	0.08	0.25	1.54	0.001	0.019	0.04	0.05	0.095	0.01	0.02	0.038	0.001	0.043

*) Internal IFE steel reference number.

Table 2. Parameters used for electrochemical measurements and calculations.

Test specimen - cylinder	10 mm \varnothing x 10 mm H, $S=3.1 \text{ cm}^2$
Linear Polarization Resistance (LPR) - R_p - sweep rate	Potential ramp -5 to +5 mV vs E_{cor} 0.1 mV/s
Electrochemical Impedance Spectroscopy (EIS)	$\pm 5 \text{ mV rms.}$, 5 kHz – 0.01 Hz
Potentiodynamic sweep -cathodic	0 to -0.3 V vs. E_{cor} , 0.1 mV/s
-anodic	0 to +0.1 V vs. E_{cor} , 0.1 mV/s
Corrosion Current Density, I_{cor}	$I_{cor} = B/(R_p S)$ B=20 mV
Corrosion Rate, v_{cor}	$v_{cor}(\text{mm/y}) = 1.16 I_{cor}(\text{Am}^{-2})$
Reference Electrode	Steel / Ag/AgCl (3 M KCl) $E = 0.194 \text{ V vs. } she$

Table 3. Equilibrium constants used in the calculations.²³⁻²⁴

Temperature/ $^{\circ}\text{C}$	80
P (CO_2) / bar	0.5
[CO_2] / mM	6.2
$\text{pK}_{1(\text{CO}_2)}$	6.23
$\text{pK}_{2(\text{CO}_2)}$	9.87
$\text{pK}_{(\text{HAc})}$	4.81
$\text{pK}_{sp}(\text{FeCO}_3)$	11.08

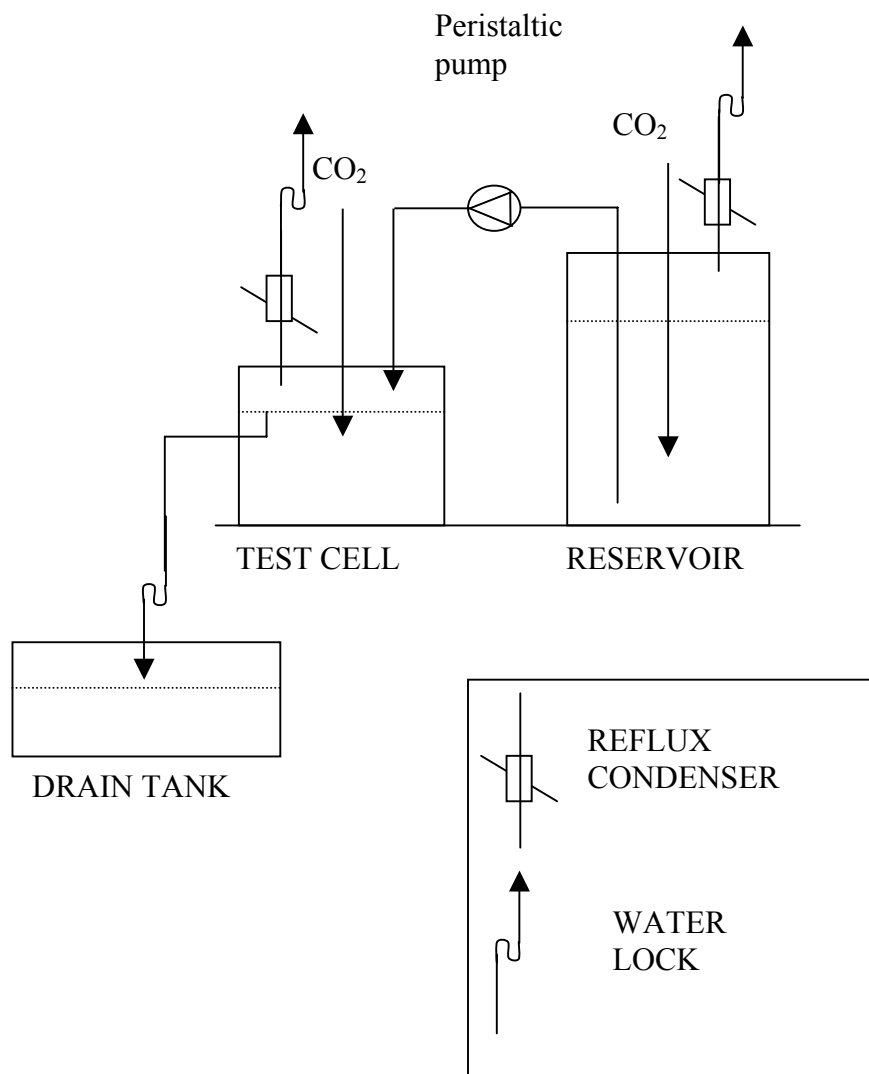
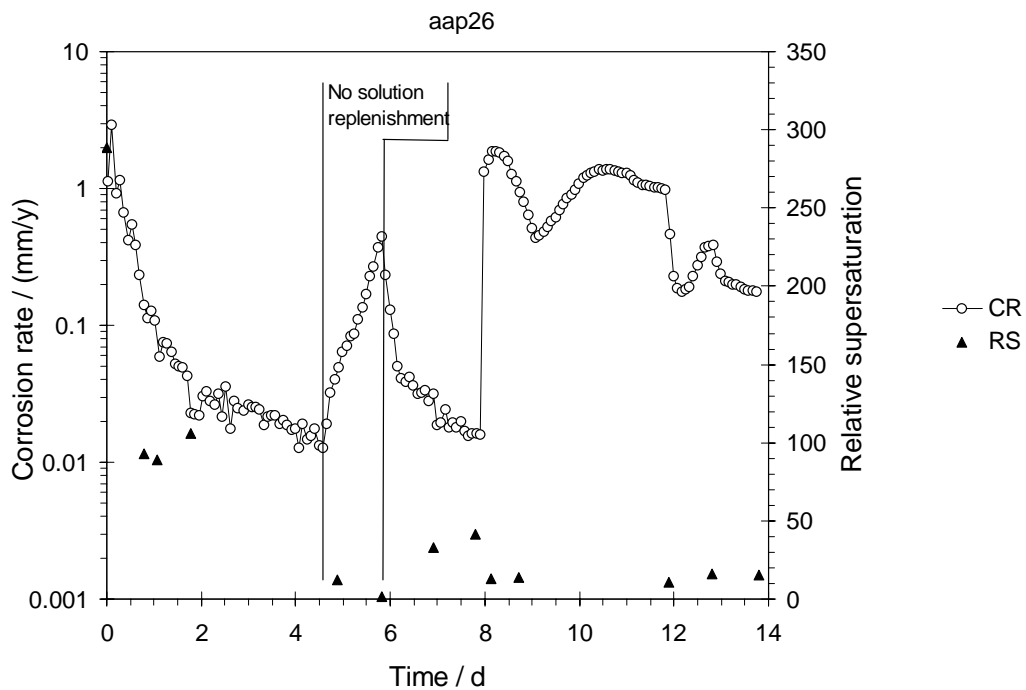


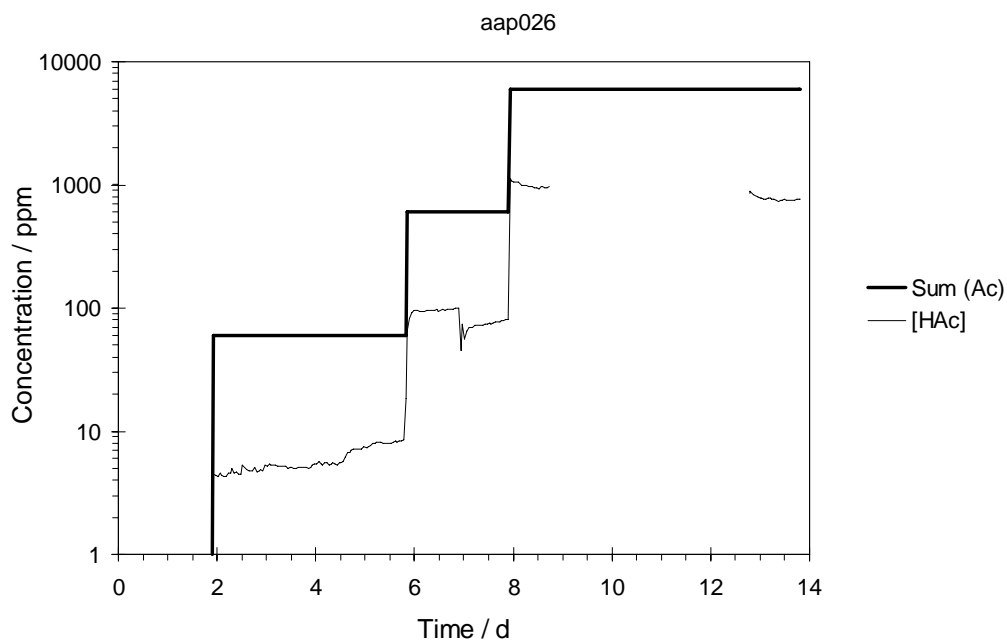
Figure 1 Schematic drawing of the test set-up in tests with rotating cylinder specimens.

Figure 2

Temp. (°C)	$\Sigma(\text{Ac})$ (ppm)	P_{CO_2} (bar)	Relative supersaturation	[NaCl] (wt%)	RCE rotation (RPM)	B_{LPR} mV
80	0-6000	0.5	280-1	0.3	100	(20)

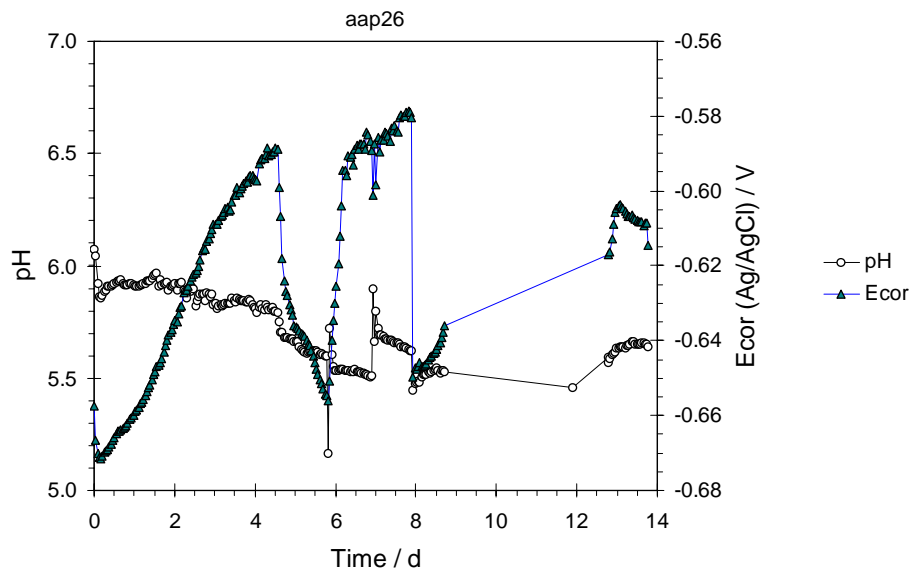


(a)

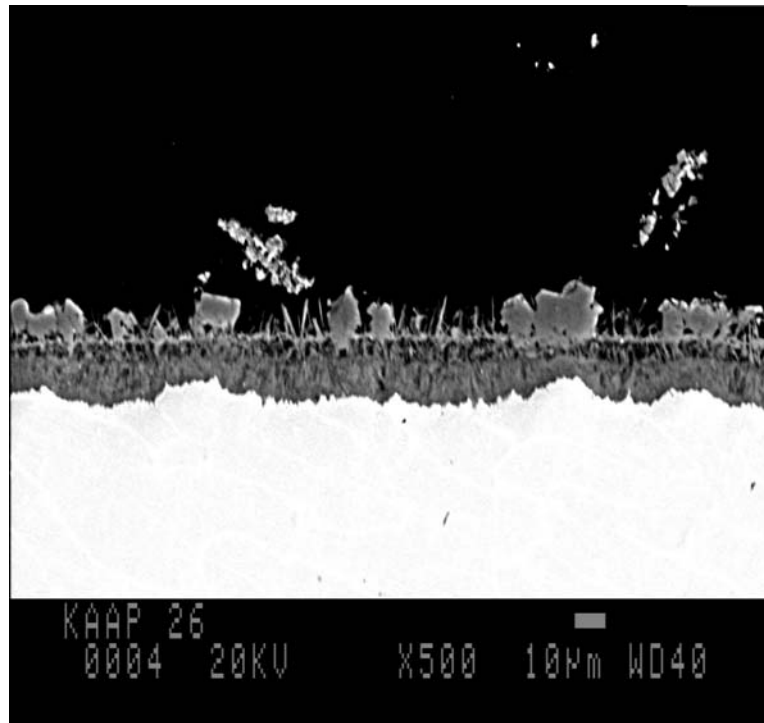


(b)

Figure 2 a-b



(c)



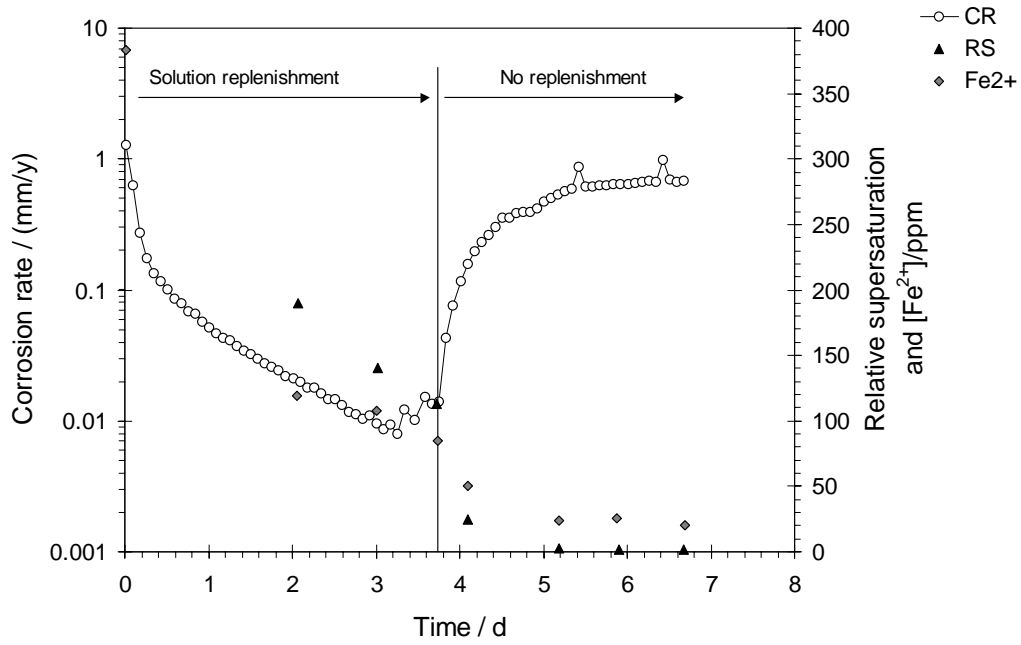
(d)

Figure 2 (a) Corrosion rate and relative supersaturation vs. time, (b) Concentration of free HAc and total acetic species vs. time, (c) pH and E_{cor} , and (d) SEM image of specimen cross section. See text for details of experimental protocol.

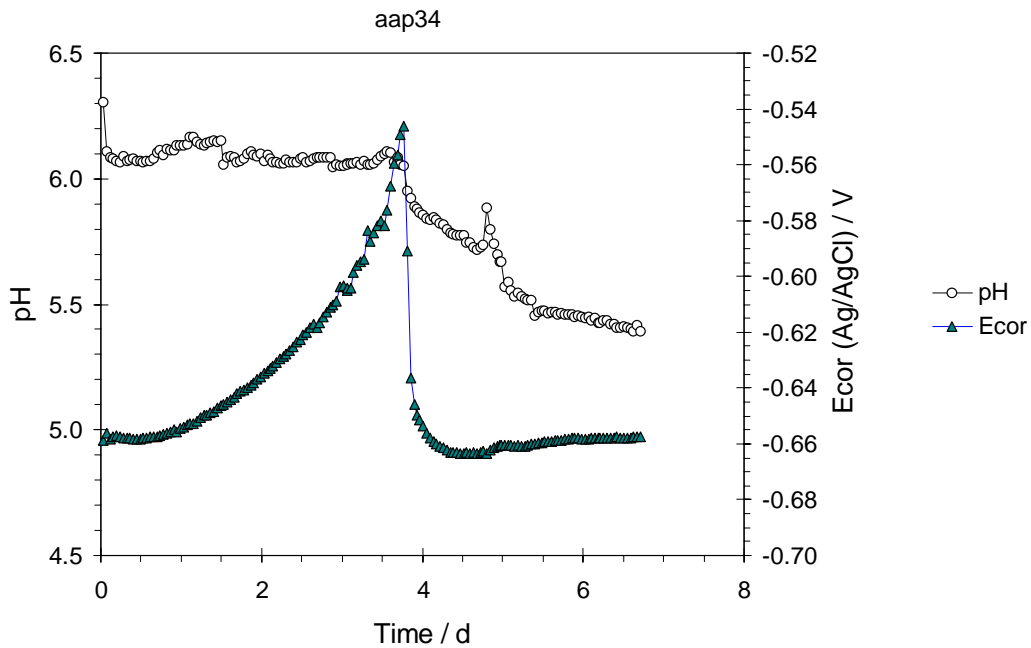
Figure 3

Temp. (°C)	$\Sigma(\text{Ac})$ (ppm)	P_{CO_2} (bar)	Relative supersaturation	[NaCl] (wt%)	RCE rotation (RPM)	B_{LPR} (mV)
80	0	0.5	200-1	0.3	100	(20)

aap34



(a)



(b)

Figure 3 a-b

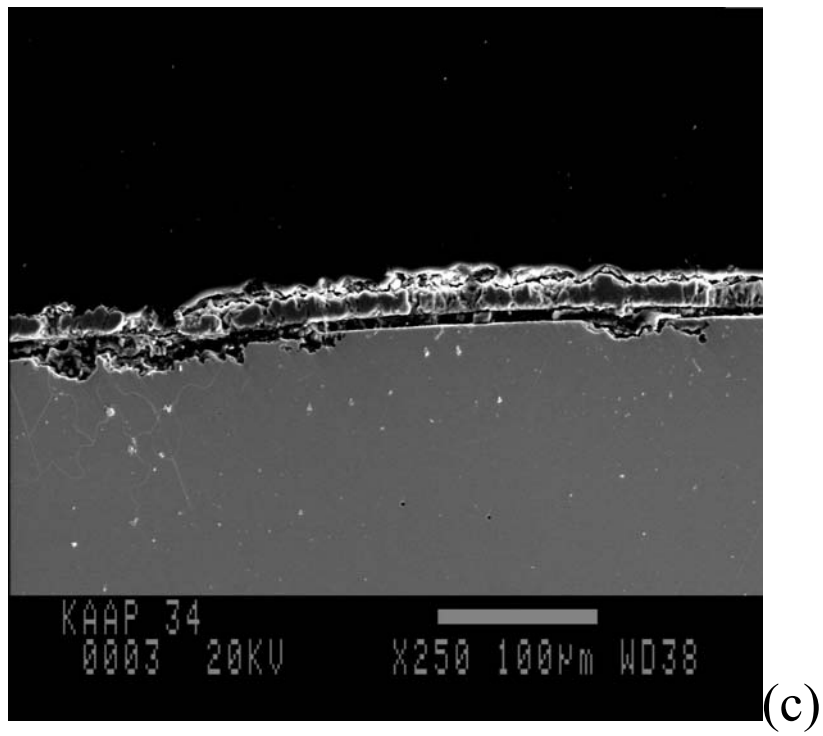
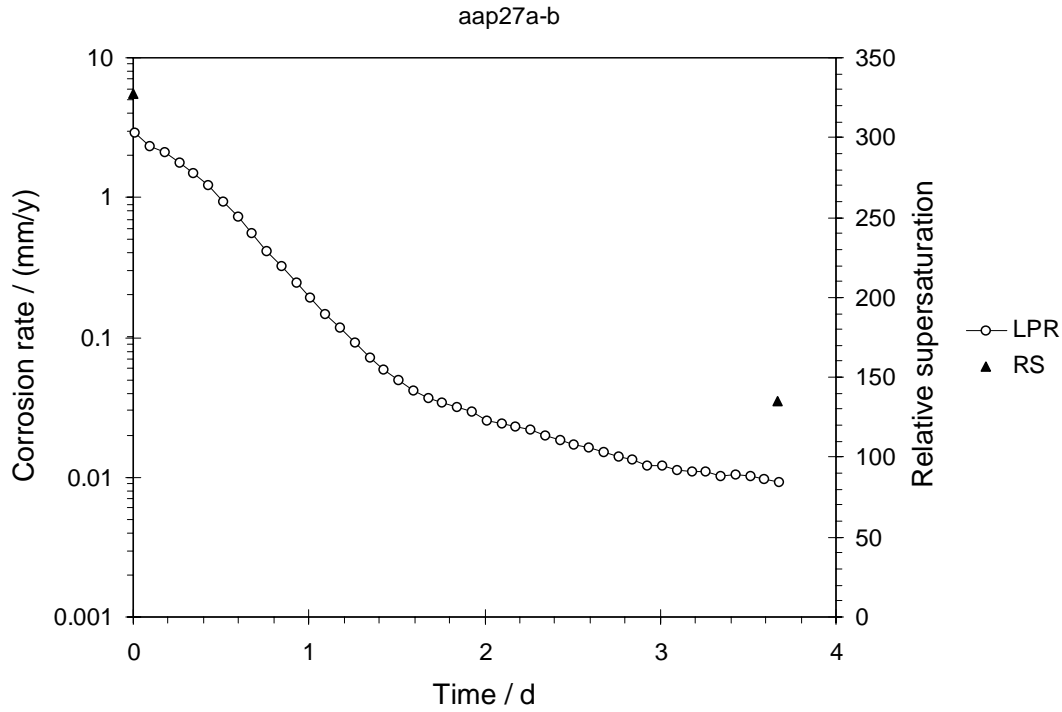


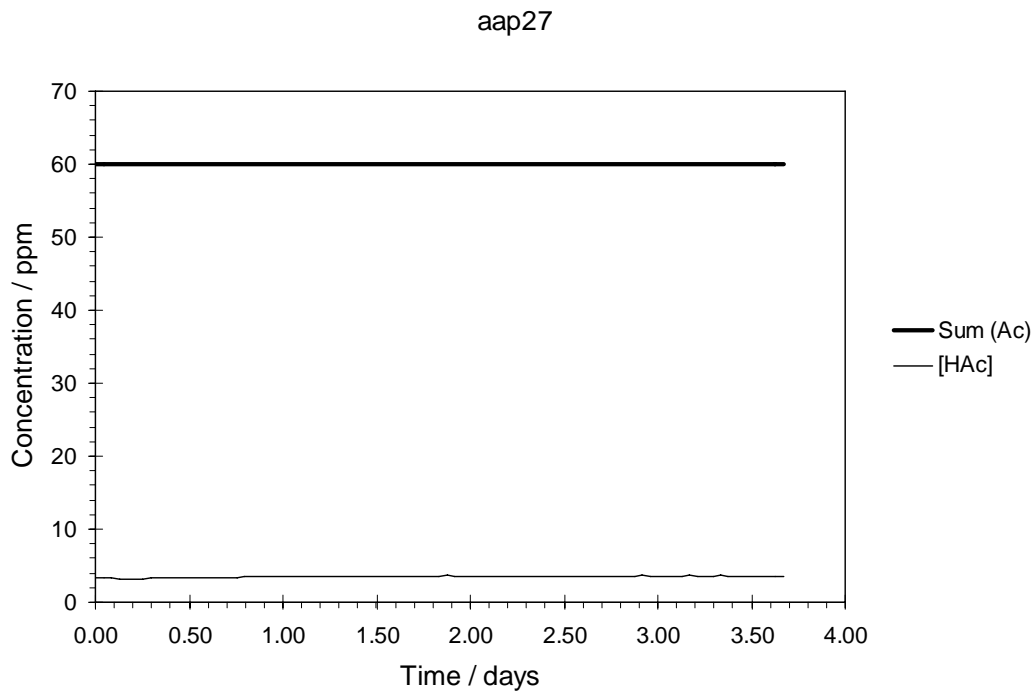
Figure 3 (a) Corrosion rate, $[Fe^{2+}]$ and relative supersaturation vs. time, (b) pH and E_{cor} , and (c) SEM image of the exposed specimen.

Figure 4

Temp. (°C)	Σ Ac (ppm)	P_{CO_2} (bar)	Relative supersaturation	[NaCl] (wt%)	RCE rotation (RPM)	B_{LPR} mV
80	60	0.5	330-135	0.3	100	(20)
Ca. 3 ppm HAc						

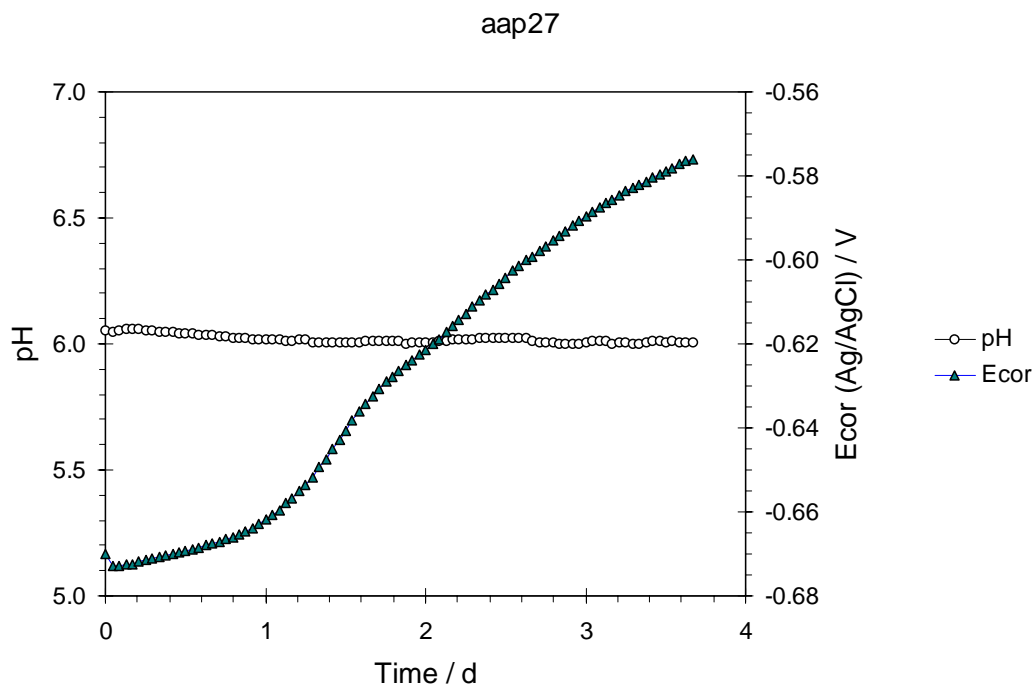


(a)

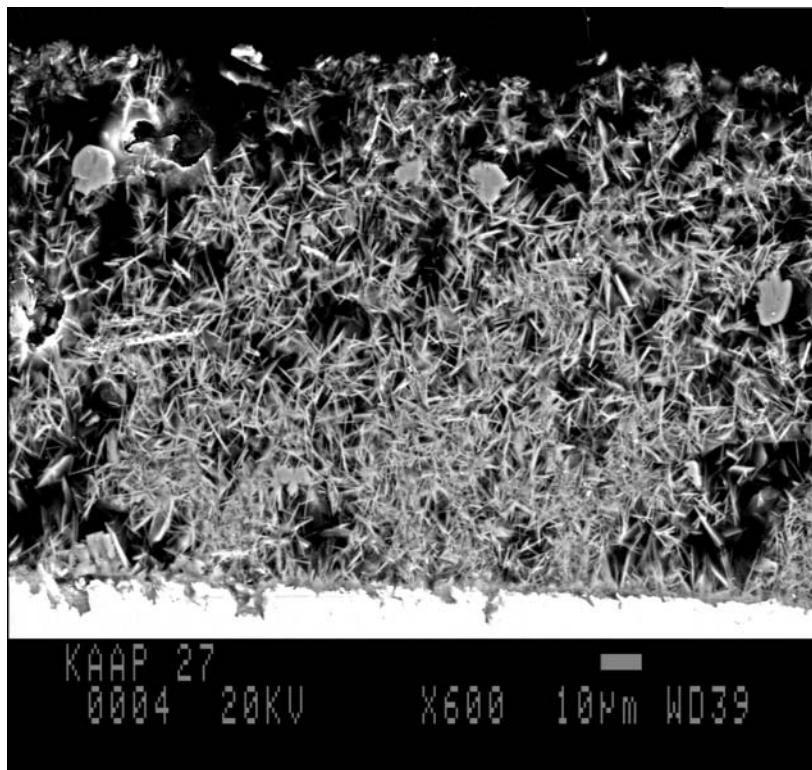


(b)

Figure 4 a-b



(c)

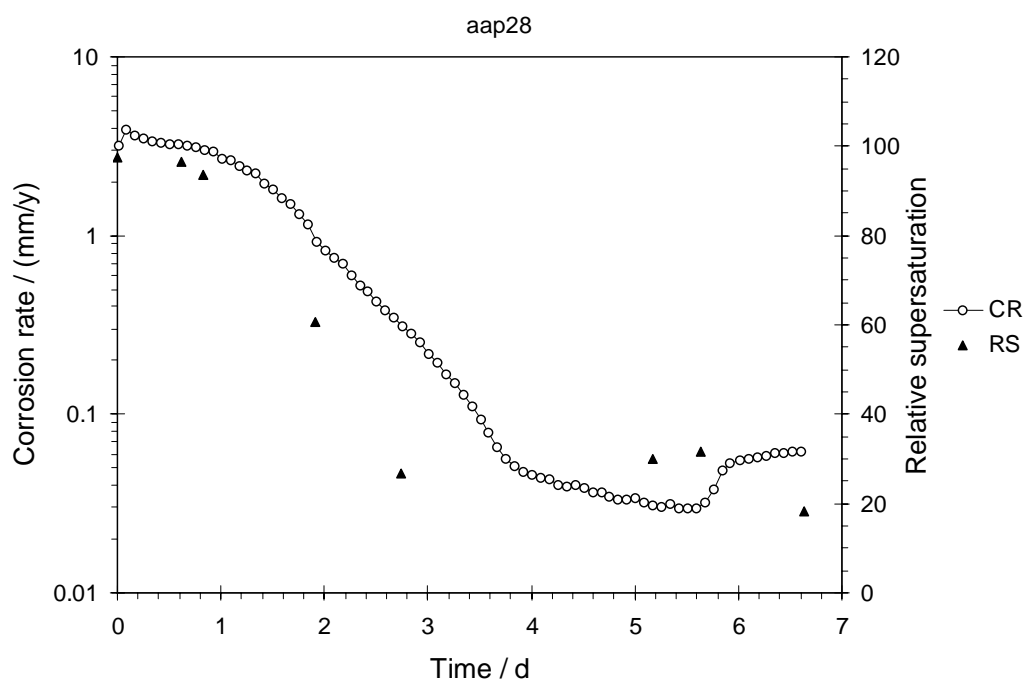


(d)

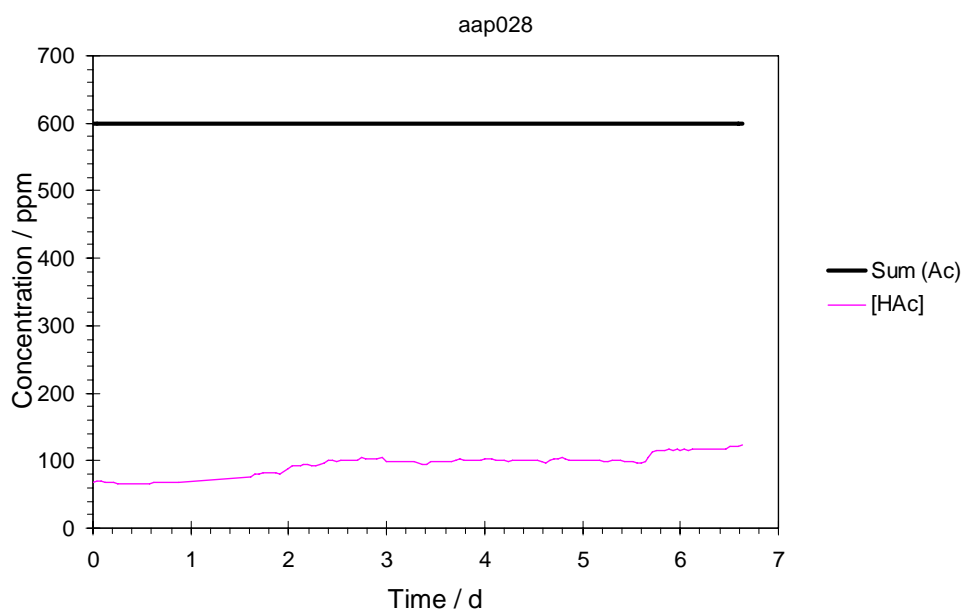
Figure 4 (a) Corrosion rate and relative supersaturation vs. time, (b) Concentration of free HAc and total acetic species vs. time, (c) pH and E_{cor} , (d) SEM image of specimen cross section.

Figure 5

Temp. (°C)	Σ Ac (ppm)	P_{CO_2} (bar)	Relative supersaturation	[NaCl] (wt%)	RCE rotation (RPM)	B_{LPR} (mV)
80	600	0.5	100-18	0.3	100	(20)
70-120 ppm HAc						

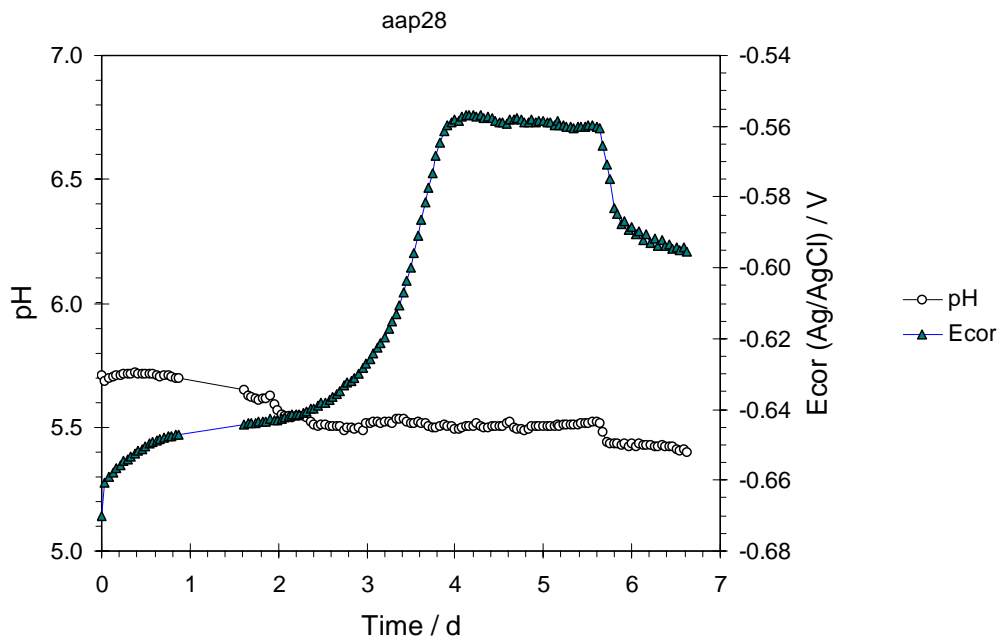


(a)

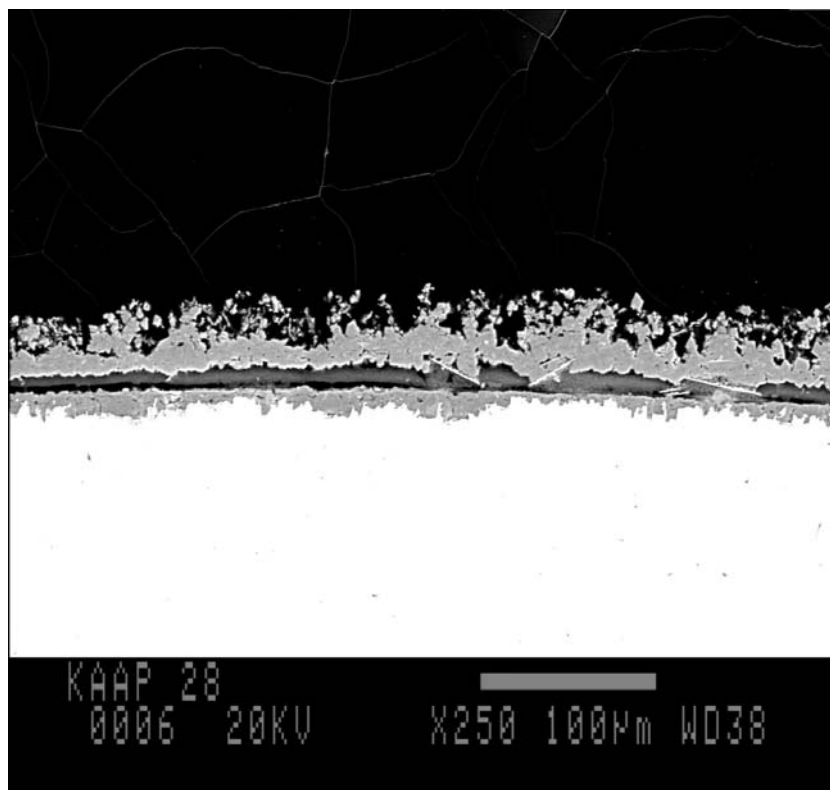


(b)

Figure 5 a-b

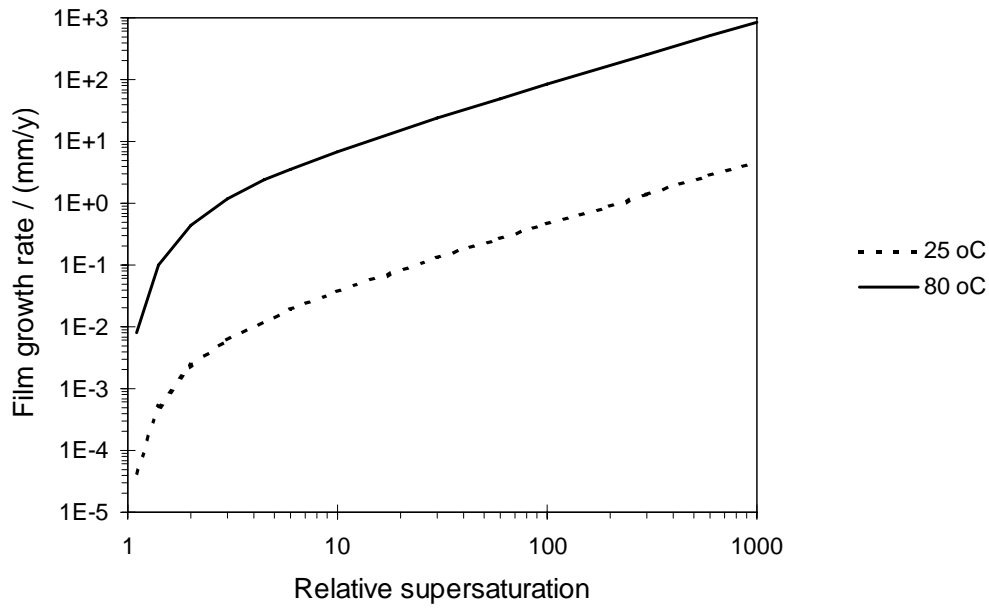


(c)

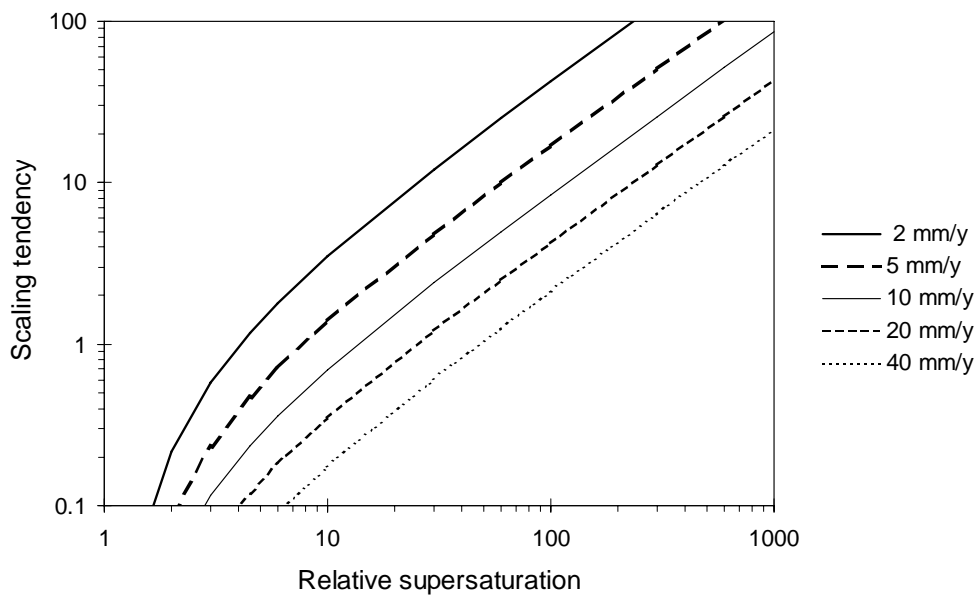


(d)

Figure 5 (a) Corrosion rate and relative supersaturation vs. time, (b) Concentration of free HAc and total acetic species vs. time, (c) pH and E_{cor} , (d) SEM image of specimen cross section.



(a)



(b)

Figure 6 (a) FeCO₃ growth rate vs. relative supersaturation at 25 and 80 °C, according to Eq. 11. (b) Scaling tendency (Eq. 12) at different corrosion rates vs. relative supersaturation at 80 °C. Calculated using FeCO₃ solubility product in Table 3 for 0.3 % NaCl solution. Supersaturation and scaling tendency is calculated for bulk solution conditions.